Physica D 238 (2009) 803–815

Contents lists available at ScienceDirect

Physica D

journal homepage: www.elsevier.com/locate/physd

Nonlinear wave–wave interactions in stratified flows: Direct numerical simulations

Yuri V. Lvov [a], Naoto Yokoyama [b,*]

[a] Department of Mathematical Sciences, Rensselaer Polytechnic Institute, Troy, NY 12180, USA
[b] Department of Mechanical Engineering, Doshisha University, Kyotanabe, Kyoto 610-0394, Japan

ARTICLE INFO

Article history:
Received 23 September 2008
Accepted 29 January 2009
Available online 12 February 2009
Communicated by A.C. Newell

Keywords:
Gravity waves
Stratified flows
Simulation

ABSTRACT

To investigate the formation mechanism of energy spectra of internal waves in the oceans, direct numerical simulations are performed. The simulations are based on the reduced dynamical equations of rotating stratified turbulence. In the reduced dynamical equations only wave modes are retained, and vortices and horizontally uniform vertical shears are excluded. Despite the simplifications, our simulations reproduce some key features of oceanic internal-wave spectra: accumulation of energy at near-inertial waves and realistic frequency and horizontal wavenumber dependencies. Furthermore, we provide evidence that formation of the energy spectra in the inertial subrange is dominated by scale-separated interactions with the near-inertial waves. These findings support observationally based intuition that spectral energy density of internal waves is the result of predominantly wave–wave interactions.

1. Introduction

Oceanic internal waves are the waves whose restoring force is buoyancy in stratified fluid. These waves are excited by flows over topography, tides and atmospheric disturbances. The energy of the waves is then transferred by nonlinear interactions among wavenumbers from large scales to small scales, and is dissipated in the small spatial scales by wave breaking. Internal waves play a significant role in the general circulation of oceans and hence the climate of the Earth.

Energy spectra of internal waves are vast with horizontal wavelengths varying from 10 m to 10^5 m, vertical wavelengths from 10 m to 10^3 m, and time periods from 10^3 s to 10^5 s.

The complexity of the internal-wave fields arises not only from its extended range of scales, but also from their interactions with the other major players in ocean dynamics including eddies, mean currents and shear flows. The main dynamical role of the internal waves is to store energy and transfer it across different scales and large distances. Hence the waves constitute a large and complex geosystem containing a broad range of interacting scales and affecting significantly most of the active players in ocean dynamics.

However, surprisingly and despite all the complexities, energy spectra of the internal waves in the oceans appear to be somewhat universal. It is given by the Garrett–Munk (GM) spectrum [1–3]. It is believed that the internal-wave spectrum may be a result predominantly, if not exclusively, of nonlinear interactions among waves.

In this paper we test the hypothesis by direct numerical simulations of the reduced model of stratified rotating turbulence. We attempted to find "universal" spectrum in our numerical simulation, perhaps similar to Garrett and Munk spectrum of internal waves in the ocean. Instead we observed strong dependency on details of numerical experiments. Nevertheless our numerical model did reproduce some key features of the oceanic internal waves

Our model contains only wave modes of stratified wave turbulence, and completely excludes vortices and horizontally uniform vertical shears. Despite these simplifications, our numerical model reproduces some key features of spectral energy density observed in the oceans.

As a result of appearance of the GM spectrum, internal waves in the ocean have been a subject of active research ever since. An important milestone was a review by Müller et al. [4]. It focuses on the resonant wave–wave interaction theory, called the weak turbulence theory. The result of the review is that the resonant wave–wave interactions in the stratified wave turbulence are dominated by specific, "named" nonlocal wave–wave interactions in the wavenumber space. The classification of the "named" nonlocal interactions appeared first in McComas [5].

Since then it was understood that in the oceans, local spectral energy density may change owing to the propagation of energy

* Corresponding author. Tel.: +81 774 65 7444.
E-mail addresses: lvovy@rpi.edu (Y.V. Lvov), nyokoyam@mail.doshisha.ac.jp (N. Yokoyama).

0167-2789/$ – see front matter © 2009 Elsevier B.V. All rights reserved.
doi:10.1016/j.physd.2009.01.016

from other parts of the ocean as well as owing to the nonlinear wave–wave interactions. A useful and intuitive diagram in the wavenumber space that separates the two regions appear in Ref. [6]. More recently, Levine [7] proposed modification of the GM spectra to take into account the dependence of the characteristic depth as a function of frequency ω. Furthermore, Lvov and Tabak [8] developed a novel Hamiltonian structure for waves in stratified flows that we use below for our numerical modeling. Historical observational data were reviewed in Ref. [9], where major deviations from the GM spectrum were categorized. Useful phenomenological characterization of fluxes of energy in internal waves were put forward by Polzin [10].

However, the GM spectrum has stood the test of time and still stands as the canonical model of the internal-wave spectral energy density. The GM spectrum is a function of the frequency ω and the vertical wavenumber m, $E(\omega, m)$. However, it is rather hard and expensive to measure the spectrum as a function of both ω and m. At least in the 1970's, when the series of the GM spectra were published [1–3], only one-dimensional spectra were generally available (with the exception of the IWEX experiment). In particular, $\overline{E}_{\text{time}}(\omega)$ was obtained from time series of mooring current meters and $\overline{E}_{\text{vertical}}(m)$ from vertical profilers. Furthermore the large wavenumber limit of $\overline{E}_{\text{vertical}}(m)$ has m^{-2} dependency.

Garrett and Munk proposed that the spectrum is *separable*, that is the product of a function of ω and a function of m:

$$E(\omega, m) \propto \overline{E}_{\text{time}}(\omega)\overline{E}_{\text{vertical}}(m). \tag{1}$$

Then $\overline{E}_{\text{time}}(\omega)$ and $\overline{E}_{\text{vertical}}(m)$ were properly normalized and chosen so that the resulting spectrum matches experimentally measured one-dimensional ω and m spectra. The resulting spectrum is given by Eq. (22) below.

The assumption of the separability allows one to construct a function of two arguments, $E(\omega, m)$ out of two one-dimensional functions, $\overline{E}_{\text{time}}(\omega)$ and $\overline{E}_{\text{vertical}}(m)$. However, if one relaxes this assumption, there is more than one way to obtain the two-dimensional spectrum, $E(\omega, m)$, to fit the observed one-dimensional spectra, $\overline{E}_{\text{time}}(\omega)$ and $\overline{E}_{\text{vertical}}(m)$. Moreover, it recently became quite apparent that the assumption (1) is not satisfied in the oceans [11]. Our numerical simulations also demonstrate that the assumption (1) is not satisfied uniformly. It also appears in our direct numerical simulations that resulting energy spectra do not display universal behavior. Rather, our simulations demonstrate accumulation of energy around the horizontally longest waves. Furthermore, we argue based on our direct numerical simulations that the energy spectrum in the inertial subrange is determined by nonlocal interactions with the accumulation. The nonlocal interaction in the wavenumber space is one of the "named" nonlocal interactions identified by McComas [5]. As a result of the nonlocal interactions, the details of behavior of the stratified wave turbulent system depends upon details of the accumulation. Consequently the resulting energy spectra are non-universal in our numerical experiments.

Despite apparent non-universality and non-separability of spectral energy density in the inertial subrange, our simulations do exhibit certain key features that are observed in the ocean. Namely, our simulations have clear peaks at inertial frequencies (horizontally longest waves) which correspond to the accumulation of energy, as observed in the ocean. Our largest numerical simulation does demonstrate the ω^{-2} dependence of the energy spectrum that appears prominently in moored observations. Furthermore our simulation demonstrate realistic k^{-2} dependence on the horizontal wavenumbers. The behavior of the spectra in the inertial subrange, formation of accumulation, apparent non-universality and violation of separability (1) can be qualitatively interpreted in terms of the nonlocal "named" interactions. These findings support observationally-based intuition that spectral energy density of internal waves is formed primarily by the nonlinear wave–wave interactions.

The stratified rotating *wave* turbulence is a subset of a much more complicated subject of rotating stratified strong turbulence governed by the Navier–Stokes equation. Complexities of the rotating stratified strong turbulence appear owing to coexistence of waves, shears and vortices and their interactions. The rotating and stratified strong turbulence have been subjects of intensive research in last few decades. Extensive numerical studies of rotating turbulence, stratified turbulence and turbulence with both rotations and stratification were performed [12–15]. Accumulation of energy at the horizontally largest scales were reported in direct numerical simulations [13,15]. The accumulation in the rotating strong turbulence happens presumably owing to the inverse cascade of two-dimensional turbulence. In contrast, in the stratified rotating turbulence, the resonant wave–wave interactions commonly cause the accumulation of energy at the horizontal largest scales.

We emphasize that the rotating stratified wave turbulence is dominated by nonlocal wave–wave interactions in the wavenumber space. Anisotropic wave turbulence systems often exhibit nonlocal interactions: drift wave turbulence, Rossby waves and MHD turbulence [16–19].

The scenario is in contrast to the local interactions of isotropic wave turbulence systems. In the locally interacting systems the spectra are insensitive to the details of large-scale and small-scale motions, and are the results of the local interactions among wavenumbers. Examples of the locally interacting systems include waves on water surfaces. In particular, universal behavior was observed in direct numerical simulations of gravity-wave and capillary-wave systems [20–24]. Note that isotropic Navier–Stokes turbulence is also widely believed to be a locally interacting system.

The paper is written as follows. In Section 2 we give the detailed description of our numerical model and assumptions used. In Section 3 we elaborate on our numerical methods, and explain pumping and damping mechanisms. In Section 4 we account for results of our numerical experiments. The formation mechanism of energy spectra is discussed in Section 5. Section 6 provides a summary.

2. Hamiltonian formalism for internal waves

In this section we provide a description of the model that we use for our numerical study. The model is based on the Hamiltonian description of the wave modes of the incompressible stratified rotating flows in hydrostatic balance. The Hamiltonian description appeared in Lvov and Tabak [8] and is presented here for completeness. Our model explicitly excludes vortices and horizontally uniform shear flows. Despite the simplification, the resulting spectrum does display some key features that are observed in the ocean.

As a starting point, we take the equations of motion satisfied by an incompressible stratified rotating flow in hydrostatic balance under the Boussinesq approximation:

$$\begin{aligned}
&\frac{\partial}{\partial t}\frac{\partial z}{\partial \rho} + \nabla \cdot \left(\frac{\partial z}{\partial \rho}\boldsymbol{u}\right) = 0,\\
&\frac{\partial \boldsymbol{u}}{\partial t} + f\boldsymbol{u}^{\perp} + (\boldsymbol{u}\cdot\nabla)\boldsymbol{u} + \frac{\nabla M}{\rho_0} = 0,\\
&\frac{\partial M}{\partial \rho} - gz = 0.
\end{aligned} \tag{2}$$

These equations are derived from mass and horizontal-momentum conservations and hydrostatic balance. The equations are written in isopycnal coordinates with the density ρ replacing the height

z in its role as independent vertical variable. Here $\boldsymbol{u} = (u, v)$ is the horizontal component of the velocity field, and $\boldsymbol{u}^{\perp} = (-v, u)$. The gradient operator $\nabla = (\partial/\partial x, \partial/\partial y)$ acts along isopycnals. The inertial frequency due to the rotation of the Earth f is assumed to be constant, g is the acceleration of gravity, and ρ_0 is a reference density (in its role as inertia) which is taken to be a constant in the Boussinesq approximation. Finally M is the Montgomery potential

$$M = P + g\,\rho\, z,$$

which is the pressure P modified by the potential energy of the stratified fluid.

The expression for the potential vorticity in these coordinates is,

$$q = \frac{f + \nabla^{\perp}\cdot\boldsymbol{u}}{\Pi}, \tag{3}$$

where $\nabla^{\perp} = (-\partial/\partial y, \partial/\partial x)$ is the two-dimensional rotation operator. Here we introduced

$$\Pi = \frac{\rho}{g}\frac{\partial^2 M}{\partial \rho^2} = \rho\frac{\partial z}{\partial \rho}$$

to be a normalized differential layer thickness. The potential vorticity is conserved along particle trajectories. Since the fluid density is also conserved along the trajectories, an initial profile where the potential vorticity is a function of the density will be preserved by the flow. Hence any chosen initial profile will stay in the fluid all the time. This observation allows us to propose that

$$q = q_0(\rho) = \frac{f}{\Pi_0(\rho)}. \tag{4}$$

Here $\Pi_0(\rho)$ is a reference stratification profile defined as

$$\Pi_0(\rho) = -\frac{g}{N(\rho)^2} \tag{5}$$

and $N(\rho)$ is the buoyancy (Brunt–Väisälä) frequency, which we shall regard as a constant N_0.

In order to separate wave and vorticity dynamics, we decompose the fluid velocity into its gradient and rotational parts, i.e.

$$\boldsymbol{u} = \nabla\phi + \nabla^{\perp}\psi. \tag{6}$$

The vorticity is derived from the potential vorticity and is distinct from the vorticity in Cartesian coordinates. In terms of the potentials ϕ and ψ, the constraint (4) reads

$$f + \Delta\psi = q_0\Pi.$$

Therefore we can express ψ as a function of Π so that Eqs. (4) and (5) are satisfied. As a result, if we redefine Π as $\Pi + \Pi_0$, Eq. (2) reduce to the pair:

$$\begin{aligned}
&\frac{\partial \Pi}{\partial t} + \nabla\cdot\left((\Pi+\Pi_0)\left(\nabla\phi + \nabla^{\perp}\Delta^{-1}\left(q_0\Pi - f\right)\right)\right) = 0,\\
&\frac{\partial \phi}{\partial t} + \frac{1}{2}\left|\nabla\phi + \nabla^{\perp}\Delta^{-1}\left(q_0\Pi - f\right)\right|^2\\
&\quad + \Delta^{-1}\nabla\cdot\left(q_0\Pi\left(\nabla^{\perp}\phi - \nabla\Delta^{-1}\left(q_0\Pi - f\right)\right)\right)\\
&\quad + \frac{1}{\rho}\int^{\rho}\int^{\rho_2}\frac{\Pi(\rho_1)}{\rho_1}\mathrm{d}\rho_1\mathrm{d}\rho_2 = 0.
\end{aligned} \tag{7}$$

The pair of Eq. (7) form a canonical conjugate pair of the Hamiltonian equations,

$$\frac{\partial \Pi}{\partial t} = -\frac{\delta \mathcal{H}}{\delta \phi}, \qquad \frac{\partial \phi}{\partial t} = \frac{\delta \mathcal{H}}{\delta \Pi}. \tag{8}$$

The Hamiltonian is the sum of kinetic and potential energies,

$$\begin{aligned}
\mathcal{H} = \int \mathrm{d}\boldsymbol{x}\mathrm{d}\rho\left(\frac{g}{2}\left|\int^{\rho}\mathrm{d}\rho'\frac{\Pi(\boldsymbol{x},\rho')}{\rho'}\right|^2\right.\\
\left. - \frac{1}{2}\left(\Pi(\boldsymbol{x},\rho) + \Pi_0\right)\left|\nabla\phi(\boldsymbol{x},\rho) + \nabla^{\perp}\Delta^{-1}q_0\Pi(\boldsymbol{x},\rho)\right|^2\right).
\end{aligned} \tag{9}$$

We therefore consider in this paper the following reduced model with the following assumptions and constraints:

- only wave motions are considered
- vortex motions are excluded
- horizontally uniform vertical shear is excluded
- potential vorticity is constrained to be constant on an isopycnal surface. Its value is determined by the underlying rotations
- constant underlying rotation f is assumed. Thus we explicitly exclude the β effect.
- hydrostatic balance is assumed.
- buoyancy frequency $N(z)$ is assumed to be constant with depth.

We do realize that the oceans are more complicated than these idealizations. Certainly for general ocean modeling the above assumptions constitute a gross simplification. The reason for our choice is that we would like to find out whether it is sufficient to study wave–wave interactions alone to determine the form of the internal-wave spectral energy density. We show below that this is indeed the case to a large extent. We show that our reduced model reproduces key characteristic behavior of the oceans. The effects of relaxing the above assumptions is the subject of future work.

3. Details of numerical methods: Implementation and interpretation

3.1. Wave turbulence

To proceed, we perform Fourier transformation and canonical transformation to the field variable, $a(\boldsymbol{p})$, defined as

$$a(\boldsymbol{p}) = \sqrt{\frac{\omega}{2g}}\frac{N_0}{|\boldsymbol{k}|}\widetilde{\Pi}(\boldsymbol{p}) - \mathrm{i}\sqrt{\frac{g}{2\omega}}\frac{|\boldsymbol{k}|}{N_0}\widetilde{\phi}(\boldsymbol{p}), \tag{10}$$

with linear coupling of the Fourier components of the stratification profile, $\widetilde{\Pi}$, and the horizontal velocity potential, $\widetilde{\phi}$. The three-dimensional wavenumber, $\boldsymbol{p}$, consists of a two-dimensional horizontal wavenumber in the isopycnal surface, $\boldsymbol{k}$, and a vertical density wavenumber, m. The linear frequency in the isopycnal coordinates is given by the dispersion relation,

$$\omega(\boldsymbol{p}) = \sqrt{f^2 + \frac{g^2}{\rho_0^2 N_0^2}\frac{|\boldsymbol{k}|^2}{m^2}}. \tag{11}$$

The usual vertical wavenumber, k_z, and the density wavenumber, m, are related as $m = -g/(\rho_0 N_0^2)k_z$.

Then, the pair of canonical equations of motion (8) is rewritten as a single canonical equation,

$$\mathrm{i}\frac{\partial a(\boldsymbol{p})}{\partial t} = \frac{\delta \mathcal{H}}{\delta a^*(\boldsymbol{p})} \tag{12}$$

with the standard Hamiltonian of three-wave interacting systems [25],

$$\begin{aligned}
\mathcal{H} = &\int \mathrm{d}\boldsymbol{p}\omega(\boldsymbol{p})|a(\boldsymbol{p})|^2\\
&+ \int \mathrm{d}\boldsymbol{p}\mathrm{d}\boldsymbol{p}_1\mathrm{d}\boldsymbol{p}_2\left(\left(V^{\boldsymbol{p}}_{\boldsymbol{p}_1,\boldsymbol{p}_2}a(\boldsymbol{p})a^*(\boldsymbol{p}_1)a^*(\boldsymbol{p}_2) + \text{c.c.}\right)\right.\\
&\left. + \left(U_{\boldsymbol{p},\boldsymbol{p}_1,\boldsymbol{p}_2}a(\boldsymbol{p})a(\boldsymbol{p}_1)a(\boldsymbol{p}_2) + \text{c.c.}\right)\right).
\end{aligned} \tag{13}$$

Here, $\delta/\delta a^*$ is the functional derivative with respect to $a^*(\boldsymbol{p})$, which is the complex conjugate of $a(\boldsymbol{p})$, and the abbreviation c.c. denotes complex conjugates of the preceding terms. The matrix elements, $V^{\boldsymbol{p}}_{\boldsymbol{p}_1,\boldsymbol{p}_2}$ and $U_{\boldsymbol{p},\boldsymbol{p}_1,\boldsymbol{p}_2}$, have exchange symmetries such that $V^{\boldsymbol{p}}_{\boldsymbol{p}_1,\boldsymbol{p}_2} = V^{\boldsymbol{p}}_{\boldsymbol{p}_2,\boldsymbol{p}_1}$ and $U_{\boldsymbol{p},\boldsymbol{p}_1,\boldsymbol{p}_2} = U_{\boldsymbol{p},\boldsymbol{p}_2,\boldsymbol{p}_1} = U_{\boldsymbol{p}_1,\boldsymbol{p},\boldsymbol{p}_2}$ [8].

The Hamiltonian (13) is the canonical form of the Hamiltonian of wave turbulence system dominated by three-wave interactions [25]. The first term describes linear noninteracting waves, the second term correspond to the nonlinear three-wave scattering processes. The wave turbulence theory provides a powerful framework to describe spectral energy transfer in the systems dominated by wave–wave interactions. A detailed review of the wave turbulence theory and its applications to internal waves is outside of the scope of the present paper, and is given in Lvov et al. [26]. Here it is sufficient to note that there are the following important classes of scale-separated resonant interactions among waves [5]:

- The vertical backscattering of a high frequency wave by a low frequency wave of twice the vertical wavenumber into a second high frequency wave of oppositely signed vertical wavenumber. This type of scattering is called Elastic Scattering (ES).
- The scattering of a high frequency wave by a low frequency and small vertical wavenumber wave into a second, nearly identical high frequency and large vertical wavenumber wave. This type of scattering is called Induced Diffusion (ID).
- The decay of a small wavenumber wave into two large vertical wavenumber waves of approximately one-half the frequency. This is called Parametric Subharmonic Instability (PSI).

This classification provides a useful interpretive framework to characterize resonant wave–wave interactions in stratified flows. We will show below that the results of our numerical simulations can be qualitatively interpreted by using this classification. Detailed theoretical analysis of scale-separated interactions of this type is presented in Lvov et al. [26]

3.2. Numerical setting

To achieve non-equilibrium statistically (near-)steady states, we have to model both processes of pumping energy to the internal-wave field and of damping energy from the field. The processes of the pumping include interactions with surface waves and tides. How to model these processes in the wavenumber space is the subject of present oceanographic research. We model the pumping processes phenomenologically. In what follows we assume that the pumping occurs on large length scales, and is relatively local in the wavenumber space. The processes that remove energy from the wave field include wave breaking, turbulent dissipation, reflection from surface and bottom boundary layers and interaction with topography. Again, the spectral details of the processes is a subject of intensive research. We assume that the processes are especially effective for small length scales (large wavenumbers).

In our numerical simulations, most of the energy provided by the external forcing accumulates around the horizontally longest waves owing to nonlinear interactions among waves. The horizontally longest waves have frequencies near the inertial frequency f. Therefore the waves are called "near-inertial waves." Then the energy is transferred through the inertial subrange, where there is no significant pumping or damping. Note that the inertial subrange therefore refers to the range in wavenumber space without effective forcing and damping, while the near-inertial waves refers to the waves with the near-inertial frequency. Subsequently energy is absorbed in the dissipation range. It is the nonlinear interactions among internal waves that determine the form of the spectrum in the inertial subrange and the formation of accumulation of energy at the near-inertial waves. The nonlinear interactions among waves is the main focus of the present paper.

In the direct numerical simulations, we add external forcing and hyper-viscosity to the canonical equation (12). Thus the dynamic equation used in the simulations is given by

$$\frac{\partial a(\boldsymbol{p})}{\partial t} = -\mathrm{i}\omega(\boldsymbol{p})a(\boldsymbol{p}) + \mathcal{N}(a(\boldsymbol{p})) + F(\boldsymbol{p}) - D(\boldsymbol{p})a(\boldsymbol{p}). \tag{14}$$

The Details of the numerical algorithm are as follows: The linear terms, i.e. a linear dispersion term and a dissipation term, $-D(\boldsymbol{p})a(\boldsymbol{p})$, are explicitly calculated. The nonlinear terms, $\mathcal{N}(a(\boldsymbol{p}))$, are derived from the nonlinear parts of the canonical equation (12) with Hamiltonian (13). They are obtained numerically by a pseudo-spectral method with the phase shift under the periodic boundary conditions for all three directions. The external forcing, $F(\boldsymbol{p})$, is implemented by fixing the amplitudes of several small wavenumbers to be constant in time. This is commonly used to simulate forcing in numerical experiments. The dissipation is modeled as hyper-viscosity:

$$D(\boldsymbol{p}) = D_{\mathrm{h}}|\boldsymbol{k}|^8 + D_{\mathrm{v}}|m|^4. \tag{15}$$

Here, D_{h} and D_{v} are chosen so that the dissipation is effective for wavenumbers larger than half of maximum wavenumber.

The wavenumbers are discretized as $\boldsymbol{p} = (2\pi/L_{\mathrm{h}}\boldsymbol{k}, 2\pi/L_{\mathrm{v}}m)$, where L_{h} and L_{v} are horizontal periodic length and vertical period in the isopycnal coordinates, and $\boldsymbol{k}$ and m are integer-valued wavenumbers. We are going to use integer-valued (dimensionless) wavenumbers from here on in this paper. Time-stepping is implemented with the fourth-order Runge–Kutta method. In all the simulations, the buoyancy frequency and horizontal period are fixed at $N_0 = 10^{-2}$ rad/s and $L_{\mathrm{h}} = 10^5$ m, respectively.

We perform a series of five numerical experiments that are listed in Table 1. The total energy per unit periodic box of all the numerical experiments except Run V is around 3×10^3 J/(kg m^2) which is characteristic of the oceans. The total energy in Run V is around 1.2×10^3 J/(kg m^2). The values of total energy density and the dissipation rate of Run V in Cartesian coordinate are 1.3×10^{-3} J/kg and 5.0×10^{-11} W/kg, respectively. These values are in good agreement with observations and theories [12].

Stratified rotating turbulence can be characterized by two dimensionless numbers, the Rossby number Ro, which is the ratio of the inertia force to the Coriolis force, and Richardson number Ri, which is the ratio of the buoyancy to the shear. They are defined as

$$Ro = \langle|(\boldsymbol{u}\cdot\nabla)\boldsymbol{u}|/|f\boldsymbol{u}^{\perp}|\rangle,$$
$$Ri = \langle N^2/S^2\rangle,$$

where $\langle\cdot\rangle$ denotes averaging in the numerical box and N and S show local buoyancy frequency given by local stratification and local shear, respectively. The values of the Rossby number and the Richardson number measured in Run V are 2.7×10^{-1} and 8.6×10^2, respectively.

3.3. Integrated and cross-sectional spectral energy density

The present paper concentrates on the investigation of the behavior of spectral energy density in the inertial subrange. As mentioned above our numerical scheme employs the pseudo-spectral algorithm. Consequently it is convenient to concentrate our attention on the (k, m) spectra. Indeed, the numerical box is a triple periodic box in the wavenumber space. On the other hand, oceanographers find it convenient to think in (ω, m) space. Indeed, the ω and m spectra could be measured experimentally.

There are merits to both ways of thinking. For example, we will demonstrate below that the spectrum is more separable in (k, m) space for Run II and III. On the other hand, Run V could be

Table 1
Numerical parameters. The wavenumbers, $\boldsymbol{k}$ and m, are discretized and they have integer values.

	Modes	f (rad/s)	L_v(kg/m^3)	Forcing	Initial condition
I	$512^2 \times 256$	$\sqrt{2}/3 \times 10^{-4}$	2.7×10	none	GM
II	256^3	0.25×10^{-4}	5.0×10	$\lvert\boldsymbol{k}\rvert^2 + m^2 \le 6^2$	White noise
III	256^3	1.0×10^{-4}	5.0×10	$\lvert\boldsymbol{k}\rvert^2 + m^2 \le 6^2$	White noise
IV	$512^2 \times 256$	$\sqrt{2}/3 \times 10^{-4}$	2.7×10	none	GM without long waves
V	$1024^2 \times 512$	$\sqrt{2}/3 \times 10^{-4}$	2.7×10	$\omega \sim 3f$	White noise

better interpreted in (ω, m) space. The oceanic spectra also tend to be more separable in (ω, m) space. Indeed, the GM spectrum is assumed to be separable in (ω, m) space. We will use both ways of thinking through the paper.

Two-dimensional energy spectra are measured in the shell of radius k as

$$E(k, |m|) = \sum_{k-1/2\le|\boldsymbol{k}'|<k+1/2} \sum_{s=\pm1} \omega |a(\boldsymbol{k}', sm)|^2. \tag{16}$$

Integrated energy spectra are defined as

$$\overline{E}_{\rm int}(k) = \sum_m E(k, |m|), \tag{17}$$

and

$$\overline{E}_{\rm int}(|m|) = \sum_k E(k, |m|). \tag{18}$$

Cross-sectional spectra, $E_m(k)$ and $E_k(|m|)$, are obtained from the two-dimensional energy spectra as a function of horizontal wavenumbers k along a certain density wavenumber m and as a function of density wavenumbers m along a certain horizontal wavenumber k, respectively.

As well as in (k, m) space, we numerically obtain energy spectra in (ω, m) space. It is made in the similar way how observational spectra are. Namely, we choose a point on the "surface" of our numerical ocean. We then conduct a "vertical mooring," recording a time series of the horizontal velocity $\boldsymbol{u}(\boldsymbol{x}_0, \rho; t)$ at a fixed horizontal position $\boldsymbol{x}_0$. The kinetic energy spectra is defined as

$$K(\omega, m) = \frac{1}{2}|\widetilde{\boldsymbol{u}}(\boldsymbol{x}_0, m; \omega)|^2, \tag{19}$$

where $\widetilde{\boldsymbol{u}}(\boldsymbol{x}_0, m; \omega)$ is the Fourier component of the horizontal velocity with respect to the vertical and time series. The integrated kinetic energy spectra $\overline{K}_{\rm int}(\omega)$ and $\overline{K}_{\rm int}(|m|)$, and the cross-sectional kinetic energy spectra $K_m(\omega)$ and $K_\omega(|m|)$ are defined from the two-dimensional kinetic energy spectrum, $K(\omega, m)$, in the same way as the energy spectra in (k, m) space.

As explained in the introduction, in the 1970's only one-dimensional spectra were widely available with the exception of the IWEX experiment. To measure $\overline{E}_{\rm vertical}(m)$ spectrum in the ocean, one can use vertical profilers at a given position. To measure $\overline{E}_{\rm time}(\omega)$ spectrum, one calculates time series of the mooring current meters. Garrett and Munk assumed that the spectrum is separable in (ω, m) space. In other words, the spectrum is the product of function of ω alone and function of m alone. In functional form, this statement is written as Eq. (1).

Then $\overline{E}_{\rm time}(\omega)$ and $\overline{E}_{\rm vertical}(m)$ were properly normalized to reproduce the characteristic total energy density of internal waves. Then these functions were chosen so that the resulting (ω, m) spectrum is consistent with both the ω spectrum and the m spectrum. In particular, the moored spectrum was chosen to be

$$\overline{E}_{\rm time}(\omega) \propto \frac{1}{\omega\sqrt{\omega^2 - f^2}}. \tag{20}$$

Notice that it has an integrable peak at the inertial frequency f. Moreover it has ω^{-2} dependence for high frequencies, as is prominently displayed in moored observations. Then the m spectrum was chosen as

$$\overline{E}_{\rm vertical}(m) \propto \frac{1}{m^2 + m^{*2}}. \tag{21}$$

Here m^* is the characteristic wavenumber determined by scale height. Detailed analysis of these choices will be presented in Polzin and Lvov [27].

The assumption of separability (1) allows one to construct a function of two arguments, $E(\omega, m)$ out of two one-dimensional functions. The resulting GM spectrum in (ω, m) space is given by

$$E_{\rm GM}(\omega, m) \propto \frac{1}{\omega\sqrt{\omega^2 - f^2}} \frac{1}{m^2 + m^{*2}}. \tag{22}$$

However, if one relaxes the assumption of the separability (1), there is more than one way to obtain the two-dimensional spectrum, $E(\omega, m)$, to fit the observed one-dimensional spectra, Eqs. (20) and (21). Moreover, it recently became quite apparent that the separability (1) is not satisfied in the oceans [11, 27]. Therefore, we could argue that reality and accuracy of the separability (1) perhaps deserves a closer examination. Furthermore, it may be possible that the one-dimensional spectra admits explanation without the separability. We therefore stress through the paper the conceptual difference between the integrated $\overline{E}_{\rm int}(\omega)$ and $\overline{E}_{\rm int}(m)$ spectra that could be confirmed by oceanographic measurements and the two-dimensional spectra which is a function of both ω and m.

A detailed analysis of the observational data is outside of the scope of the present paper. We will present such analysis in Polzin and Lvov [27]. There details of IWEX and other experiments will be presented and reanalyzed. We will also present there results and analysis of more modern observations. A brief catalog of historically available observational programs in the past three decades, along with characterization of deviations from the GM spectrum, is available in Lvov et al. [9].

The linear dispersion relation (11) links ω and m with the horizontal wavenumber k. With the linear dispersion relation, the spectrum can be transformed from both wavenumber space, (k, m), into frequency–horizontal-wavenumber space, (k, ω), or frequency–vertical-wavenumber space, (m, ω). In particular, the GM spectrum in (k, m) space is given as

$$\begin{aligned} E_{\rm GM}(k, m) &= E_{\rm GM}(\omega, m)\frac{\partial\omega}{\partial k} \\ &\propto \frac{1}{f^2 + \frac{g^2}{\rho_0^2 N_0^2}\frac{|\boldsymbol{k}|^2}{m^2}} \frac{1}{|m|\left(m^2 + m^{*2}\right)}. \end{aligned} \tag{23}$$

Note that in this form, the spectrum (23) is *not* separable, i.e. can not be represented as a product of function of k and function of m. By using Eq. (23) we can define the integrated m spectra,

$$\begin{aligned} \overline{E}_{\rm int,GM}(m) &= \int_f^{N_0} E_{\rm GM}(\omega, m)\mathrm{d}\omega \\ &= \int_0^{\frac{\rho_0^2 N_0^2}{g^2}|m|\sqrt{N_0^2 - f^2}} E_{\rm GM}(k, m)\mathrm{d}k. \end{aligned} \tag{24}$$

In the large-wavenumber and large-frequency limit, Eq. (22) has the self-similar asymptotic form given by

$$E_{\mathrm{GM}}(\omega, m) \propto \omega^{-2}|m|^{-2}. \tag{25}$$

Similarly, in the large-wavenumber limit, Eq. (23) has a form

$$E_{\mathrm{GM}}(k, m) \propto k^{-2}|m|^{-1}. \tag{26}$$

Both Eqs. (25) and (26) should give the same one-dimensional spectrum as a function of vertical wavenumbers,

$$\overline{E}_{\mathrm{int,GM}}(m) \propto |m|^{-2}. \tag{27}$$

The difference between the exponents of m in Eqs. (26) and (27) comes from the non-separability of Eq. (23) in the (k, m) space.

Note that the power-law exponents of one-dimensional spectra and those of two-dimensional cross-sectional spectra do not have to coincide. Indeed, the exponents of the integrated spectra are a *weighted* mean of those of the cross-sectional spectra, as seen in Eqs. (17) and (18). Note, however, that for the separable spectrum the the exponents of the integrated spectra coincide with those of the cross-sectional spectra.

4. Numerical results

4.1. Run I

Since the GM spectrum was believed to be the universal oceanographic spectrum up to a certain degree, the natural question to ask is whether the GM spectrum could be a steady state of our numerical wave model. We realize that such a guess may be far-fetched, but it is nevertheless appealing to check it. Therefore we are led to examine the statistical stability of the GM spectrum. We assume that the steady state of the ocean can be characterized by an energy flux from pumping regions to damping regions in the wavenumber space. Therefore to achieve a truly steady state we need to model both pumping processes and damping processes. As explained above, in modeling the damping we use the traditional hyper-viscosity approach in Eq. (15). As we will see below, the resulting spectrum depends upon the large-scale flows. Therefore, the only way to see whether the GM spectrum is close to being a steady state that is independent of the form of the pumping is to choose no pumping at all. Thus we are led towards modeling the system as a freely decaying system, i.e. without external forcing.

The GM spectrum with the cut-off in large horizontal and density wavenumbers is employed as the initial energy spectrum. The cut-off is introduced to avoid decreasing accuracy of the pseudo-spectral method. The initial phases of complex amplitude, $a(\boldsymbol{p})$, are given by uniformly distributed random numbers in $[0, 2\pi)$.

Fig. 1 shows the initial spectrum and the energy spectrum after about 35 h in ocean time. If the GM spectrum were to be a universal steady state of our numerical model, it would change very little in this simulation. Instead, the density exponents rapidly change from -1 to -2 only after 1.5 days. This spectral change occurs faster than dissipation effects with timescale estimated to be about 50 days at $|m| = 32$. Therefore it appears that the GM spectrum is not a stable universal spectrum in the wavenumber region $16 < |m| < 64$ at least for this particular numerical experiment. The behavior of this numerical experiment appears to contradict the arguments of McComas [5], McComas and Müller [28] based on the induced diffusion approach that all energy spectra are rapidly relaxed to the GM spectrum, but is consistent with Winters and D'Asaro [12].

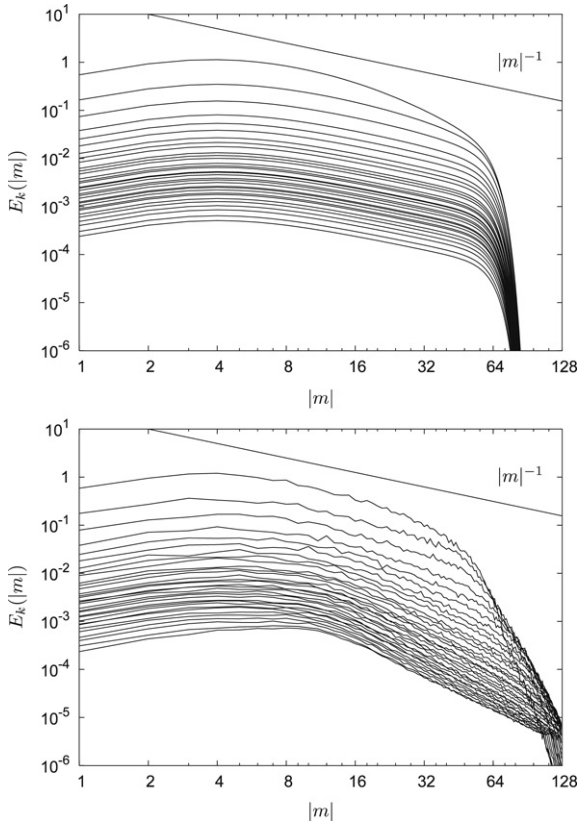

Fig. 1. Cross-sectional spectra $E_k(|m|)$ of GM spectrum as the initial condition (top) and of energy spectrum after about 35 h (bottom) of Run I. Significant differences in the region $16 < |m| < 64$ indicates that GM spectrum is not statistically steady.

4.2. Run II and III

We certainly realize that our numerical model of Run I does not fully describe the ocean. Then we question what could be the nature of the statistical steady state of our wave model of stratified rotating turbulence. Here we model the pumping phenomenologically. We assume that waves are forced at horizontally and vertically large scales, i.e. small wavenumbers. In particular we choose the forced wavenumbers such that

$$|\boldsymbol{k}_{\mathrm{F}}|^2 + |m_{\mathrm{F}}|^2 \le 6^2. \tag{28}$$

The forcing is modeled by fixing the amplitude of the forced wavenumbers to be constant in time. We also added an additional external dissipation $-D_\omega(\omega - N_0)^2$ for $\omega > N_0$ in these runs to avoid violation of the hydrostatic balance. Detailed investigation of the non-hydrostatic effects is outside of the scope of present paper.

Since the energy flows in the wavenumber space strongly depend on the inertial frequencies f (Ref. [29]), we performed Run II and III with differing values of the inertial frequencies f (see Table 1). For Run II, the inertial frequency $f = 0.25 \times 10^{-4}$ rad/s, while for Run III the value of the inertial frequency is $f = 1 \times 10^{-4}$ rad/s. These inertial frequencies correspond to latitudes of 10 degrees and 45 degrees.

Note that there is a "critical" latitude where the frequency of the semidiurnal tide is equal to twice the inertial frequency. The principal difference between these two runs is that Run II is southwards of "critical" latitude in the northern hemisphere while Run III is northwards.

Our phenomenological forcing (28) corresponds to the band of frequencies greater than $4f$ for Run II and $\sqrt{2}f$ for Run III. These values are the result of the discreteness of the numerical grid. Certainly the forcing is not necessarily characteristic of the

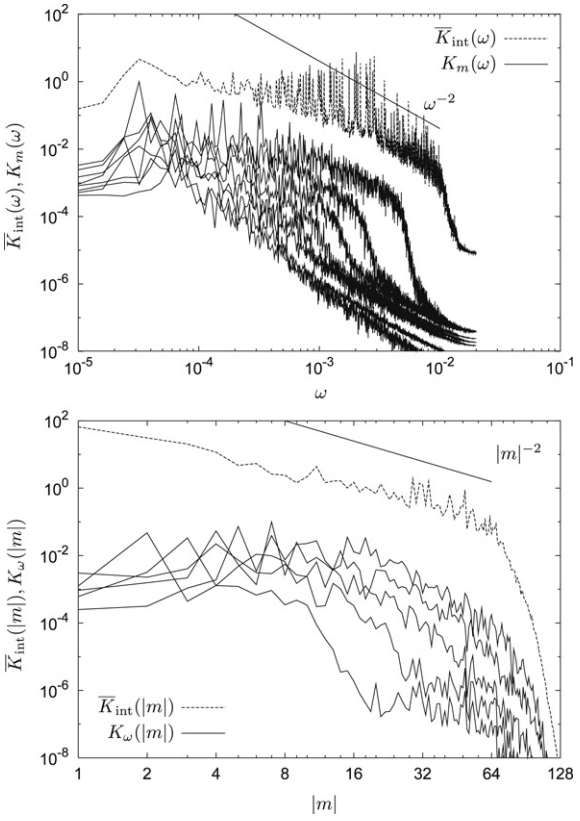

Fig. 2. Integrated kinetic energy spectra $\overline{K}_{\rm int}(\omega)$ and $\overline{K}_{\rm int}(|m|)$, and cross-sectional energy spectra $K_m(\omega)$ and $K_\omega(|m|)$ of Run II. The kinetic energy spectra are obtained as functions of ω and m from time and vertical series of the horizontal velocity $\boldsymbol{u}(\boldsymbol{x}_0, \rho; t)$. The GM spectrum scales as $\omega^{-2}|m|^{-2}$ for large frequencies and density wavenumbers. The cross-sectional spectra that are functions of frequencies (top) are shown every eight curves for visibility. The cross-sectional spectra that are functions of vertical wavenumbers (bottom) are shown when $\omega = 2, 4, 8, 16, 32 \times 10^{-4}$ rad/s.

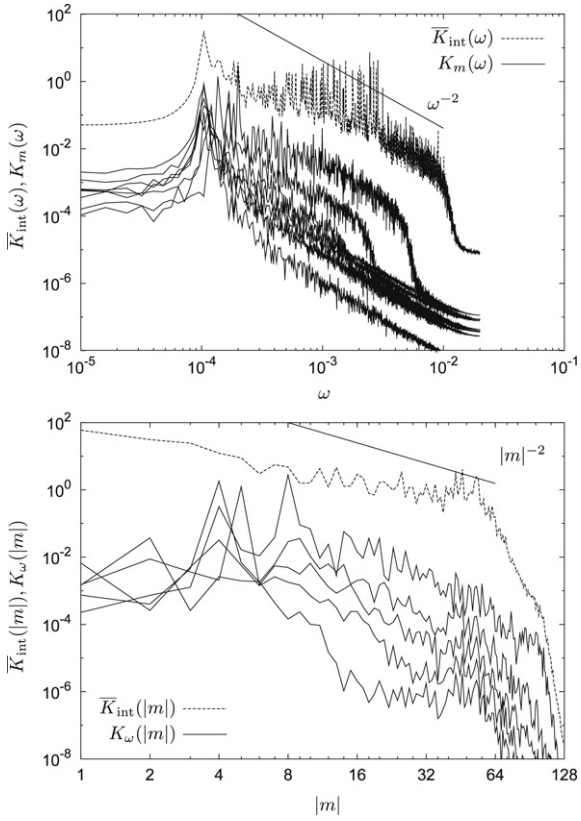

Fig. 3. Integrated kinetic energy spectra, and cross-sectional energy spectra of Run III. See the caption of Fig. 2 for details.

ocean and is purely phenomenological, and chosen for numerical simplicity and to allow easy interpretation.

The kinetic energy spectra as functions of ω and m of Run II and III are shown in Figs. 2 and 3. Both frequency spectra (top in Figs. 2 and 3) have peaks at the inertial frequencies. This indicates that most energy accumulates in the near-inertial frequencies. This behavior is characteristic of the ocean. Indeed, these peaks correspond to the integrable singularity at the inertial frequency of the GM spectrum (22).

After about 10^3 days from the initial time when all the wavenumbers have extremely small energy, the systems are still transient and the accumulation of energy in the near-inertial frequencies has not reached a complete statistically steady state. Thus the timescale of the development of the accumulation is relatively large. Consequently one may conjecture that other processes, not present in our numerical model may affect the ocean at large timescales. The most important of such processes which is not included in our simulations are the β effects. Indeed, inclusion of β effects would lead to existence of Rossby waves in our simulation, which may alter our results significantly. Other effects not present in our simulations, which can affect larger scales, may also alter the results. However, this paper focuses on the investigation of the energy spectrum formation in the inertial subrange, rather then on the energy spectra in the large-scale flows. For this purpose, our numerical model is consistent with observationally-based intuition that wave–wave interactions is the predominant mechanism of forming the internal-wave spectrum in the inertial subrange.

The energy spectrum of Run II has only weak accumulation of energy in the near-inertial frequency. This could be qualitatively explained by the fact that all the forced wavenumbers have frequencies greater than $4f$ for Run II. Consequently, PSI is effective in transferring energy to frequencies around $2f$ and large vertical wavenumbers. Then PSI can no longer be effective in transferring energy towards the accumulation of energy in the near-inertial frequencies. Indeed, second PSI transfer would make the vertical wavenumber much larger and thus would move away from the accumulation. On the contrary, the energy spectrum of the Run III has moderate accumulation, stronger than that of Run II. This could be explained by the fact that the forced modes have frequencies greater than $\sqrt{2}f$. Then PSI can be effective in transferring energy from the wavenumbers that have frequency $2f$ to the accumulation whose frequencies are close to f (Ref. [29]).

Since the forcing does not have just one frequency but several frequencies, the integrated spectra $\overline{K}_{\rm int}(\omega)$ have huge oscillations corresponding to the linear frequencies of the forced wavenumbers. Therefore, the power-law region of the frequencies, $10^{-4} \lesssim \omega \lesssim 10^{-2}$, are strongly affected by the forcing. However, the cross-sectional spectra with $|m| > 6$ are not much affected by the forcing.

It is difficult to analyze cross-sectional vertical-wavenumber spectra (bottom in Figs. 2 and 3). Indeed, these spectra do not appear to be separable, i.e. can not be represented by product of two one-dimensional functions, as in Eq. (1). Moreover, these cross-sectional spectra do not appear to exhibit self-similarity, or power-law patterns. On the other hand, the integrated spectra do exhibit self-similarity. Therefore it appears that integrated spectra can perhaps be interpreted without separability. Also notice that the integrated spectra of the vertical wavenumbers are strongly affected by he peaks at the near-inertial frequencies. Consequently, integrated spectra are determined by the large scale

Fig. 4. Integrated energy spectra $\overline{E}_{\rm int}(k)$ and $\overline{E}_{\rm int}(|m|)$, and cross-sectional energy spectra $E_m(k)$ and $E_k(|m|)$ of Run II. The GM spectrum scales as $k^{-2}|m|^{-1}$ for large horizontal and density wavenumbers. The cross-sectional spectra are shown every four curves for visibility.

Fig. 5. Integrated and cross-sectional spectra of Run III. See the caption of Fig. 4 for details.

flow. Therefore, the cross-sectional spectra and the integrated spectra describe internal waves from different perspectives.

It appears that it is advantageous to obtain (k, m) spectra as well. The integrated energy spectra, $\overline{E}_{\rm int}(k)$ and $\overline{E}_{\rm int}(|m|)$, and cross-sectional energy spectra, $E_m(k)$ and $E_k(|m|)$, of Run II and Run III are shown in Fig. 4 and in Fig. 5, respectively. Note that these figures can roughly be interpreted as being composed of almost parallel lines. Thus these figures indicate that the energy spectra as functions of k and m appear to be more separable than the kinetic energy spectra as functions of ω and m in Run II and III.

To elaborate on this point, we measure the power-law exponents of the cross-sectional spectra. These power-law exponents of the cross-sectional spectra are determined by the least-squares fit as

$$E_m(k) \propto k^{\alpha(|m|)} \quad \text{in } k \in [8, 40]$$

and

$$E_k(m) \propto |m|^{\beta(k)} \quad \text{in } |m| \in [8, 40].$$

The power-law exponents of the integrated spectra are also obtained as

$$\overline{E}_{\rm int}(k) \propto k^{\alpha_{\rm int}}$$

and

$$\overline{E}_{\rm int}(|m|) \propto |m|^{\beta_{\rm int}}$$

in the same wavenumber regions. The resulting power-law exponents of the integrated and cross-sectional spectra are shown in Figs. 6 and 7.

Note that in Run II the energy spectrum appears to be close to double-power

$$E(k, m) \propto k^{-2}|m|^{-2.5} \tag{29}$$

in the large horizontal and density wavenumbers.

Fig. 6. Power-law exponents of each cross-sectional spectrum in Run II. top: $\alpha(|m|)$, which are the exponents of the cross-sectional energy spectra $E_m(k)$, bottom: $\beta(k)$, which are the exponents of the cross-sectional energy spectra $E_k(|m|)$. The error bars are obtained by fitting errors due to the least-squares method. The exponents of the integrated spectra are also shown.